Calculation of a Hollow-Cone Liquid Spray in a Uniform Airstream

G. J. Sturgess,* S. A. Syed,† and K. R. McManus‡
United Technologies Corporation, East Hartford, Connecticut

A spray model is used to calculate a spray formed by a hollow-cone, pressure-atomizing, swirl-jet fuel injector spraying water downward in a vertically mounted wind tunnel passing a coflowing uniform airstream. Two sets of initial boundary conditions for the origins of the liquid spray were explored in the calculations. The first set provided characteristic initial velocities and angles of trajectory for each droplet size range at breakup of the fuel sheet issuing from the atomizer. The second set provided random sampling of droplets in size, velocity, and angles within the limits established by the measurements. It is concluded that the spray model, when used with the stochastic approach to initial conditions for the liquid phase, is sufficiently encouraging to continue investigations of its performance.

Introduction

FLUID dynamic computer codes are being developed for the mathematical simulation of flows in gas turbine engine practical combustion systems. The codes are desired as design, diagnostic, and development tools.

One viscous flow code that has seen widespread acceptance in the fluid dynamics community is the so-called TEACH code. This code originated at Imperial College, London, England, as a teaching aid.[1]

The viscous flow codes currently used by Pratt & Whitney (P&W) grew out of the generic TEACH solution procedure. For P&W use it is necessary to validate such codes. Code validation is best carried out in systematic fashion by comparison of code calculations against benchmark-quality experiments in order to explore the performance of the physical modeling embodied in the calculation procedure.

In order to calculate an aircraft gas turbine combustion chamber, the computer code should include a model for the liquid fuel spray.[2] The performance of the spray model is extremely important because, in conjunction with the turbulence model, it determines the distribution of fuel in the burning zone of the combustor. The model must calculate the spray characteristics accurately because they can also act as additional rate-controlling parameters in the overall heat release process.

Spray Modeling

The trajectories of the liquid droplets produced by the spray atomizer were calculated as they traversed the gaseous flowfield. This method involves embedding the droplet equations of motion in Lagrangian form into the Eulerian framework of the gas-phase equations. A fuel droplet can then be tracked through the gaseous flowfield. This treatment was formulated by Megdal and Agosta.[3]

An instantaneous quantity, ϕ, in a gaseous turbulent flow, is described as the sum of a time-averaged value $\bar{\phi}$ and a randomly fluctuating value ϕ'. This description is substituted into the Navier-Stokes equations which are valid at any instant of time, and these are time-averaged. The resulting equations, simplified by neglecting fluctuations of laminar viscosity and density, are known as the Reynolds equations. The Reynolds equations are algebraically manipulated into a general form. Following the approach of Crowe[4] and Buckingham and Siekhaus[5] the gaseous phase is coupled to the liquid phase by incorporating a void fraction term Ω into the general flow equation. For example, for two-dimensional steady flow, and using cylindrical coordinates,

$$\frac{\partial}{\partial x}(\bar{\rho}_g \Omega \bar{u}_g \bar{\phi}) + \frac{\partial}{r\partial r}(r\bar{\rho}_g \Omega \bar{v}_g \bar{\phi}) = \frac{\partial}{\partial x}\left(\Omega \Gamma_{\text{eff},\phi} \frac{\partial \bar{\phi}}{\partial x}\right) + \frac{\partial}{r\partial r}\left(r\Omega \Gamma_{\text{eff},\phi} \frac{\partial \bar{\phi}}{\partial r}\right) + S_{\Omega,\phi} + S_{d,\phi} \quad (1)$$

where

ϕ = any of the dependent variables
$\Gamma_{\text{eff},\phi}$ = an appropriate turbulent exchange coefficient, depending on what ϕ represents
$S_{\Omega,\phi}$ = source term for gaseous phase
$S_{d,\phi}$ = droplet source term

and the subscript g denotes the gaseous phase.

For $0 < \Omega \leq 1$, the gas phase responds to the presence of the droplets. The droplet source term $S_{d,\phi}$ is obtained by calculating the loss or gain of droplet mass, momentum, energy, etc., within each computational cell of the Eulerian finite difference grid through which the droplet passes. This is known as the "particle source in cell" (PSIC) method[3,6,7] where the droplet source terms identify the contribution of the droplets.

Auxiliary equations define a computational "droplet," its location, and its change of state. The spray model provides these equations.

In the spray model the spray is represented by individual droplets, termed "computational droplets." This is Crowe's discrete droplet model.[4] Each computational droplet represents a "parcel" of like droplets all having the same initial size, velocity vector, and temperature. All of the droplets in a real spray are represented by a size distribution; the Rosin-Rammler distribution is computationally convenient. The calculated spray size distribution representing the actual

Presented as Paper 84-1322 at the AIAA/SAE/ASME 20th Joint Propulsion Conference, Cincinnati, OH, June 11-13, 1984; received Aug. 10, 1984; revision submitted April 9, 1985. Copyright © American Institute of Aeronautics and Astronautics, Inc., 1984. All rights reserved.

*Senior Research Engineer, Pratt & Whitney Engineering Division. Member AIAA.
†Research Engineer, Pratt & Whitney Engineering Division.
‡Analytical Engineer, Pratt & Whitney Engineering Division.

spray is sampled statistically to produce the computational droplets; real fuel-flow rate is maintained at its correct value. The computational droplets are then fired into the gas field.

The droplet equation of motion is due to Soo,[8] with his simplifying reductions and the assumption that the fuel vapor produced by the evaporating droplet has an initial velocity equal to that of its droplet. This yields

$$m_d \frac{\mathrm{d}u_{d,i}}{\mathrm{d}t} = m_d F_i (u_{g,i} - u_{d,i}) + m_d g_i \tag{2}$$

where

$$F_i = \frac{3}{8} C_D \frac{\rho_g}{\rho_d r_d} |(u_{g,i} - u_{d,i})| \tag{3}$$

and

$u_{d,i}$ = droplet velocity in the x, r, and θ directions, respectively, i.e., u_d, v_d, and w_d when Eq. (2) is rewritten in cylindrical coordinates
r_d = droplet radius (droplets assumed spherical)
C_D = drag coefficient (relationship of Williams[9])
ρ = density

Then, the droplet position at any instant of time is given by

$$\frac{\mathrm{d}x}{\mathrm{d}t} = u_d, \quad \frac{\mathrm{d}r}{\mathrm{d}t} = v_d, \quad r\frac{\mathrm{d}\theta}{\mathrm{d}t} = w_d \tag{4}$$

Use of the Lagrangian approach makes the treatment of turbulent diffusion of droplets difficult. Turbulence models for two-phase flows are being developed,[10] but result in extremely complicated equations to be solved. Turbulent diffusion of droplets is accounted for herein by a stochastic approach.[11] In the droplet equation of motion, Eq. (2), $u_{g,i}$ is interpreted as the instantaneous value of the gas velocity, i.e.,

$$u_{g,i} = \bar{u}_{g,i} + u'_{g,i} \tag{5}$$

as before. The time-mean value $\bar{u}_{g,i}$ is obtained from the gaseous flowfield solution. The instantaneous value $u_{g,i}$ can be obtained using random sampling of an assumed Gaussian probability distribution function for turbulence energy, together with the assumption that the turbulence is isotropic. The standard deviation of $u_{g,i}$ is then

$$\sigma = (\tfrac{2}{3}K)^{1/2} \tag{6}$$

where K is the specific kinetic energy of turbulence available throughout the field from the gas-phase solutions. The fluctuating velocity $u'_{g,i}$ then can be obtained from the definition of K and Eq. (5). Hence,

$$u_g = \bar{u}_g + u'_g, \quad v_g = \bar{v}_g + u'_g, \quad w_g = \bar{w}_g + u'_g$$

The time interval over which the droplet equations of motion are integrated is the time a particular instantaneous velocity interacts with the droplet. To determine this time interval, it is assumed that an instantaneous velocity is associated with a particular turbulent eddy. The droplet interacts with the eddy until either the droplet traverses the eddy or it is captured by the eddy and the eddy is broken up, whichever occurs first. The length scale of the eddy is obtained from the turbulence model (in this case, the two-equation or K-ϵ model) as

$$\ell_T = C_\mu K^{3/2}/\epsilon \tag{7}$$

where ϵ is the dissipation rate of K and C_μ a constant equal to 0.09. The transit time t_t is determined analytically from a simplified and linearized form of the droplet equation of motion as

$$t_t = \frac{4}{3} \frac{\rho_g D_d^2}{\mu_g Re,_d C_D} \ell n \left[1 - \ell_T \left(\frac{3}{4} \frac{\mu_g Re,_d C_D}{\rho_d D_d^2} \div \left| \left(u_{d,i} - u_{g,i} \right) \right| \right) \right] \tag{8}$$

where

$$Re,_d = \rho_g D_d |(u_{g,i} - u_{d,i})|/\mu_g$$

The derivation of Eq. (8) is too long to be given here.

When the logarithm in Eq. (8) becomes negative, there is no solution and the droplet is assumed to be captured by the eddy. The interaction time t_i is then equal to the eddy lifetime t_e, which can be estimated from

$$t_e = \ell_T / |u'_{g,i}| \tag{9}$$

Hence,

$$t_i = \min (t_t, t_e) \tag{10}$$

The droplet source terms in Eq. (1) involve, for each computational cell of the finite difference grid upon which this equation is solved, the following droplet and gas exchanges:

1) Mass transfer (continuity equation), $S_{d,m}$
2) Momentum transfer (momentum equations), $S_{d,u}$, $S_{d,v}$, $S_{d,w}$
3) Enthalpy exchange (energy equation), $S_{d,h}$
4) Species exchange (specie equation), $S_{d,ml}$
5) Radiation exchange (energy equation), $S_{d,R}$

Expressions for these source terms may be written.[4]

The void fraction is given by

$$\Omega = 1 - \frac{4\pi}{3V} \sum_{L=1}^{N} \left[\frac{1}{M} \sum_{K=1}^{M} (D_d^3 \dot{n}_L t_L)_K \right]_L \tag{11}$$

where $\dot{n}_L$ is the number of real droplets per unit time in size range L crossing cell; M the number of droplets representing size range L; N the total number of size ranges representing spray; and V the cell volume. The overall solution is obtained by iterating between the calculations of the two phases until convergence is reached.

Phenomenological modeling of the heat-transfer and evaporation processes is used to provide closure. For example, the well-known empirical correlations for isolated droplets, as given in Ref. 12.

In a disperse spray the droplets can have significant mass in comparison to the gaseous phase because of the large density differences that can exist. Thus, the droplets can still influence the gaseous phase, and this is adequately accounted for through the droplet source terms and the inclusion of void fraction Ω in Eq. (1). Very dense sprays can also modify the turbulence of the gaseous phase[10]; however, this is not presently accounted for.

Spray calculation procedures such as those described have been used in calculating reacting flows in combustors,[13-15] however, these studies have compared measurements of the reacted flow against overall calculations, so that it is not possible to separate the performances of the separate physical models used. Studies of spray formation in a gas turbine combustor were made by Boysan et al.,[16] however, the results were not compared against spray measurements. None of the studies referred to above accounted for dispersion of the droplets by gas-phase turbulence. The stochastic approach to turbulent dispersion of droplets[11] is receiving systematic investigation by Shuen et al.[17,18,20,21] and Solomon et al.[19,22]

The present investigation differs from Shuen and Solomon's investigations in two aspects: 1) the spray studied is injected from a practical pressure atomizer and, therefore, does not have well-defined or controlled initial conditions; and 2) the spray is enclosed and injected into a coflowing environment.

Experimental Data

To evaluate the spray model, an experiment was selected from the literature. The available choices were not many,[2] but the experiment of Mellor et al.[23] performed at Sheffield University some years ago seemed the most suitable for an initial study.

The experiment consisted of a 30.5×30.5-cm cross-sectional wind tunnel with a bellmouth intake drawing air from the atmosphere. An air velocity of 14.7 m/s was established in the working section, with the velocity uniform across the tunnel. A swirl-spray pressure atomizer was mounted centrally on a slender sting aligned with the tunnel axis to spray vertically downward. The atomizer had a flow number of 5.42 (lb/h$\sqrt{\text{psi}}$) and sprayed 24.57 kg/h of water with a measured cone angle of 84.4 deg. The Sauter mean diameter (SMD) of the spray was measured as 91.8 μm.

The operating conditions for the experiment and the use of ambient temperature water as the liquid sprayed meant that evaporation was negligible for the distances at which measurements were made. Experience with wind tunnels similar to the one used suggested that turbulence intensities of 2-3% or less could be expected in the working section. Turbulent dispersion of the droplets should not be large at such conditions. Therefore, the experiment is ideally suited for examining the behavior of the droplet equations of motion. The provision of considerable information at the liquid sheet break-up plane also permits a study to be made of the effects of different boundary condition treatments for the liquid phase on the calculated results.

Calculation Grid

In the TEACH solution procedure a hybrid finite differencing scheme is used that results in stable and realistic solutions. The scheme selects central differencing to calculate convective and diffusive fluxes across cells formed by the calculation grid when the absolute value of the cell Peclet number is less than or equal to 2; otherwise, upwind differencing is used for convective fluxes and diffusive fluxes are neglected. Although upwind differencing improves numerical stability, it introduces a diffusion-like term into the difference equations that results in numerical diffusion of the convected parameter.

For the flow to be calculated, convection strongly dominates streamwise diffusion, and there is negligible streamline curvature and streamline-to-grid skewness. Therefore, excessive grid refinement to reduce the cell Peclet numbers was not felt to be necessary.

The experiment was three-dimensional in nature to provide high-quality optical access for the photographs. It was modeled using a two-dimensional (axisymmetric) representation. This was done for reasons of solution economy, and to retain the axisymmetric character of the liquid spray issuing from the spin chamber of the fuel injector, without the use of a curvilinear coordinate system in the calculation.

The diameter of the circular duct representing the wind tunnel was taken as the hydraulic diameter of the actual working section. The atomizer dimension, and, hence, the spray origin, was small in comparison to that of the duct. Therefore, the influence of the flow boundaries on the initial region of spray development was acceptably small. The calculation domain was taken to extend to 36 cm from the fuel injector, and the radius of the duct was 15.26 cm.

The calculation domain was one-half of the duct and filled with a nonuniform grid consisting of 30 mesh lines in the streamwise direction and 20 mesh lines in the cross-stream direction.

Boundary Conditions

Boundary conditions have to be supplied for the gaseous and liquid phases to make the calculation.

Gas Phase

For those cells formed by the grid that fall along the borders of the calculation domain, the values of the variable ϕ are specified as input boundary conditions. Due to the elliptic nature of the equations being solved, it is necessary to include the outlet as a boundary.

Along solid surfaces the no-slip condition was assumed, and wall boundary layers were represented through wall functions based on Couette flow. For the inlet representing the tunnel inflow, the uniform axial velocity of 14.7 m/s was used, and radial and tangential velocities were taken as zero. The turbulence intensity $u'_{\text{rms}}/\bar{u}$ was assumed to be 1.5%. For a turbulence length scale, 3% of the tunnel hydraulic diameter was used. The turbulence intensity is used to calculate the inlet value of the specific kinetic energy of turbulence K. The turbulence length scale ℓ_T is used with Eq. (7) to determine the dissipation rate of K. (Away from the inlet, transport equations are solved for K and ϵ.)

The duct was modeled as being axisymmetric about the centerline of the fuel injector. On the axis of symmetry the radial velocity was taken as zero, as were the gradients of all of the other variables. At the outlet, all gradients were assumed to be zero; axial velocity was corrected to conserve an integral mass balance after applying the zero velocity gradient condition.

Liquid Phase

The origin of the spray was taken as the end of the liquid sheet. This was found to be 0.3 cm axially downstream and at a radius of 0.28 cm. The sheet velocity at breakup was 34 m/s and its half-angle was 42.2 deg. The break-up region extended to about 1 cm downstream from the injector. In the break-up region the sheet formed ligaments and subsequently drops. At the end of the break-up region only the very largest drops (200 μm) were not spherical. For the break-up region, 1200 drops were analyzed in the experiment, and information was provided relating drop number/size/velocity and drop number/size/angle of trajectory; unfortunately, the relationships between drop velocity and angle were not given.

The information on the break-up region was presented[23] graphically. Data were extracted from the graphs using a digitizer. The extracted data were used to provide boundary conditions for the liquid phase. Two approaches were used: 1) statistical organization to produce a single characteristic velocity and angle of trajectory for each drop size range, and 2) a stochastic approach to account for the probability that in a given size range droplets could acquire more than a single angle and velocity. Both approaches were assumed to apply to the end of the liquid sheet position.

At a calculation boundary a droplet can be either reflected or remain on the boundary. If it remains on the boundary it is taken out of the calculation. If it is reflected, new initial velocity conditions are specified. This means that the sign of the velocity component normal to the boundary is altered, and tracking is resumed. A droplet is only reflected when it crosses an axis of symmetry. A droplet is taken out of the calculation when the boundary is a solid wall.

Characteristic Initial Conditions for Droplets

To illustrate the technique, two droplet sizes will be presented. A total of 59 droplets of 60 μm diameter exist for which velocity was measured at this size. The frequency distribution of data appears to be nearly normal. This was so

for droplets in the 60-90-μm range; however, for both lower and higher drop sizes the distributions are skewed and, in some cases, suggest two populations. The percentage cumulative relative frequencies were therefore plotted in the useful Weibull probability form.

Figure 1 shows the Weibull probability plot for the 60-μm droplets. The data yield a linear relationship with a slope of 6.25. A slope equal to 3.44 is a Weibull distribution approximating a normal distribution, so that the present distribution is therefore more sharply peaked and is skewed to the right compared to a normal distribution. The characteristic velocity is taken as the 63.2 percentile point. Thus, for the 60-μm droplets, the characteristic velocity was obtained as 28 m/s.

The procedure described above was repeated for a number of drop sizes, and the resulting characteristic velocities are presented against drop size in Fig. 2. Shown on the figure are velocities representing the fuel sheet at breakup and the air velocity into which the spray is introduced. The mean line drawn through the derived data points asymptotically approaches the liquid sheet velocity for very large drops, and falls to the air velocity as the droplets approach zero size. This is the expected behavior.

A similar procedure was followed for droplet angles of trajectory to produce the characteristic angle plot of Fig. 3. In producing this figure, for example, the histogram for 80-μm droplets was made from 28 samples and clearly suggests the existence of two populations. The corresponding Weibull probability plot given in Fig. 4 shows neither a straight line nor a smooth curve, but exhibits a discontinuity. Such a discontinuity is indicative of two populations in the sample. This feature was typical for all of the angle data. The delineation between the two populations can be seen to exist for trajectories lesser and greater than the fuel sheet angle of 42.2 deg. The correct way to proceed would be to identify the cause of the two populations, separate the data by cause, and replot separately for each population.

Due to the nature of Fig. 4, a possible assumption could be that the 80-μm droplets with angles greater than that of the liquid sheet originate from the outer surface of the sheet, and that those with angles less than that of the sheet originate from its inner surface. Figure 4 of Ref. 23, which shows a photograph of the edge of the break-up region, suggests that this is not an unreasonable assumption. If the data sample is separated according to this assumption, good linear Weibull probability plots result, and the two characteristic trajectory angles are obtained. These are 48-deg half-angles for angles greater than the liquid sheet, and 34.4 deg for angles less than the liquid sheet angle.

It is worthwhile to examine if the distribution of drops across the break-up region is skewed. If the total data for all drop sizes is partitioned by angle into groups with angles less than that of the liquid sheet and angles greater, the number of droplets in each class of data are about equal, with 55.3% of the drops having angles less than the fuel sheet. The histograms for the two classes show that the size distributions are different. Weibull probability plots reveal that, of the droplets with angles greater than that of the fuel sheet, 50% have diameters less than 65.4 μm. However, for those droplets with angles less than that of the fuel sheet, only 8.7% have diameters less than 65.4 μm. Thus, although the sheet produces about the same number of droplets on the inside as on the outside of the spray, there are less smaller drops on the inside of the spray than on the outside. This can also be seen when the variation of mean drop size across the spray is examined, as in Fig. 5. The mean drop diameter is defined as

$$\bar{d} = \frac{\Sigma(n_i d_i)}{N_\alpha} \tag{12}$$

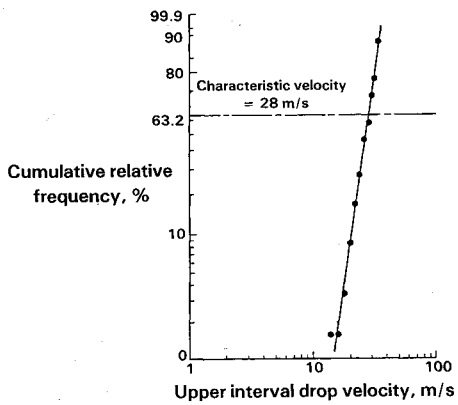

Fig. 1 Weibull probability plot for initial velocity of 60-μm droplets.

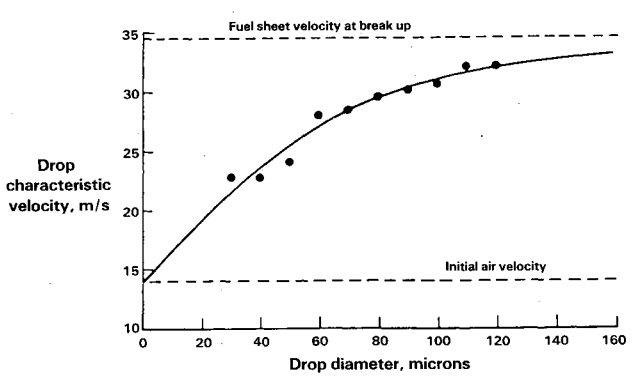

Fig. 2 Characteristic velocities for all droplets at liquid sheet breakup.

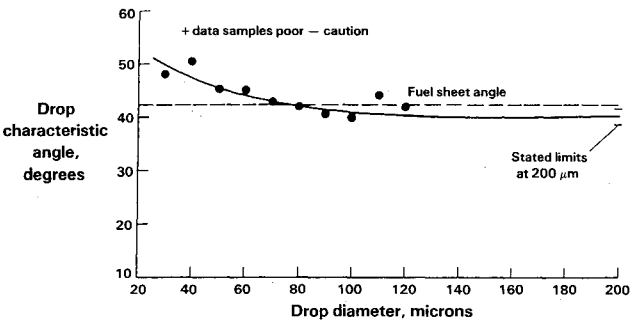

Fig. 3 Characteristic angles for droplets at breakup.

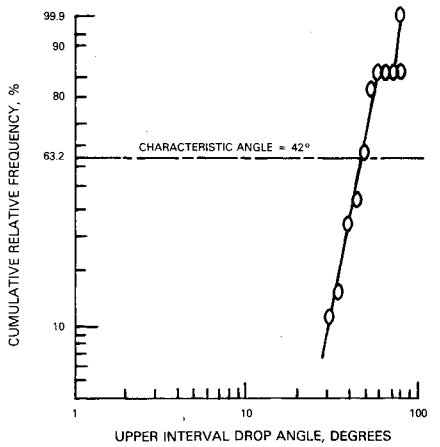

Fig. 4 Weibull probability plot for angle of trajectory for 80-μm droplets showing two populations at breakup.

where d_i is the mean of the drop size range, n_i the number of drops in the size range at the angle, and N_α the total number of drops in the angle size range.

Figure 5 suggests that the mean drop size is roughly constant on the outside of the spray, but increases nearly linearly toward the injector centerline on the inside.

Physically, the greater number of smaller drops and lower mean drop size on the outside of the spray could be due to the direct action of the coflowing airstream on breakup of the liquid sheet outer surface. This action is not present on the inner liquid surface.

The implication of these findings on the nonuniform and nonsymmetrical nature of the break-up region is that the use of a single characteristic angle for each drop size is really not a very realistic approach to describing droplet initial conditions.

Stochastic Initial Conditions for Droplets

A stochastic approach to droplet initial conditions was considered, which takes into account the likelihood that a given drop size range requires more than a single velocity and angle to adequately represent its contribution to the spray distribution.

For each drop size range four velocities and angles were selected. These were distributed across the measured data range about the characteristic velocities and angles in a more or less arbitrary manner. Since the relationships between velocity and angle were not given in Ref. 23, all possible combinations of the four selected angles and velocities were used, yielding 16 different initial conditions for each size range. Ten drop size ranges were used from 40 to 220 μm in uniform 20-μm intervals. Table 1 gives the initial conditions thus obtained. There is no relation between the velocities and angles of trajectory given.

The origin of the computational spray was based on a total of 160 drops, constructed from Table 1. For each of the 16 combinations of angle and velocity possible for a given drop size in Table 1, the u_d and v_d velocity components were established as input data for the computer program. It was assumed here that w_d was zero, although the atomizer produced the liquid sheet from a swirl chamber. Droplets from such injectors do not seem to have a swirl component when observed, although the liquid sheet may have one. The random number generator of the computer was used to select the implied pairing of angle and velocity from this input data. This was done for each drop size range in a sampling that was weighted according to the percentage of total injected fuel associated with a given drop size. This was obtained from the cumulative volume distribution measured for the complete spray and reported in Ref. 23. In this manner, conservation of liquid mass for the spray was preserved. After 1000 computational droplets had been selected and fired into the flowfield, the random input arrangement of drop velocity components in a size range was shuffled for all size ranges, and this shuffling was repeated after another 1000 droplets. This was done to ensure true randomness in the sampling. Thus, the spray was built up from a total of 3000 computational droplets produced in this fashion.

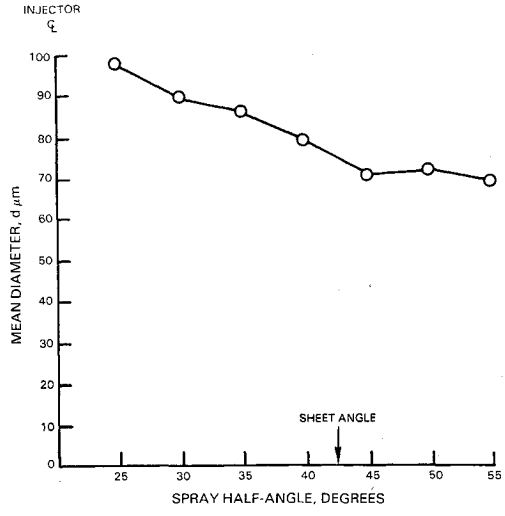

Fig. 5 Variation of mean drop size across break-up region showing bigger drop size on inside of spray.

The 3000 droplets used to obtain the data presented were introduced into the initially converged two-phase calculation at a rate of 50 per iteration, so that the total number of droplets used in the whole calculation was on the order of 5000.

The procedure described should result ideally in a Gaussian distribution of fuel across the break-up region. The distribution would be expected to be symmetrical about an angle that depended on the original choice of angles given in Table 1.

The foregoing stochastic procedure for droplet input conditions goes part-way to address the shortcomings inherent in the characteristic velocity/angle approach. It does cover drop velocity vs angle relationships reasonably adequately. However, it is applied in random fashion across the break-up region. It does not account in this form for the observed nonuniformity of droplets across the break-up region, illustrated in Fig. 5.

To establish the nonuniformity of the break-up region quantitatively, the local droplet distributions were determined as a function of angle of trajectory. This was done by fitting a computationally convenient Rosin-Rammler distribution to the measured data at a number of angles, i.e.,

$$R = \exp\,[-(d/\bar{d})^n] \tag{13}$$

where R is the cumulative volume of drops greater than diameter d, expressed as a ratio of total volume of the sample; and $\bar{d}$,n are constants to be determined.

At each angle, droplet numbers were counted for ± 2.5 deg about the nominal value. The resulting values of n and $\bar{d}$ are given in Fig. 6 as a function of nominal angle, and show remarkable consistency with angle variation. These values define the change in droplet distribution with position, and

Table 1 Droplet initial conditions for stochastic approach

Drop size range, μm	Droplet angle, deg	Droplet velocity, m/s	Drop size range, μm	Droplet angle, deg	Droplet velocity, m/s
40	58	28	140	47	34
	46	24		45	32
	39	20		40	31
	30	17		35	29
60	55	32	160	45	34
	46	28		43	33
	39	24		41	31
	29	19		38	30
80	53	32	180	44	34
	45	29		43	33
	39	26		41	32
	30	23		39	31
100	50	33	200	42	34
	45	30		41	33
	40	28		40	32
	30	25		39	31
120	49	33	220	41.5	34
	44	31		41	33.5
	39	29		40.5	32.5
	32	27		40	32

relate to the liquid sheet breakup. It is interesting to note that Simmons[24] quotes values of n as being between 2 and 4 for most sprays. For comparison, the appropriate values of n and $\bar{d}$ for the entire spray across the complete break-up region were 3.23 and 123, respectively. The distribution given as Eq. (13) was not as good a representation as it was on a local basis. This was because of the previously noted population differences between the inside and outside of the spray.

The fuel distribution across the break-up region was also found by dividing the measured volume of droplets at a nominal angle by the total volume of all droplets counted for the break-up region. It can be seen from Fig. 7 that there is more fuel on the inside of the spray than on the outside, and that the majority of the fuel is confined to angles greater than 25 deg and less than 55 deg. The hollow-cone character of the spray is seen.

Figures 6 and 7 provide the necessary information for a more sophisticated stochastic procedure for droplet input conditions that accounts for the skewness in the real droplet distributions at breakup.

Although the original stochastic representation of droplet initial conditions was intended to be a random approach, consideration of Table 1 reveals that the minimum droplet initial angle inadvertently was held roughly constant at about 30 deg for the droplet size range from 40 to 120 μm. This truncated the distribution and resulted in a fuel distribution across the break-up region that was rather different from that given in Fig. 7, and did not match the cumulative volume distribution measured for the break-up region. To correct this biasing and to account for the nonuniform distribution of droplet sizes across the break-up region, the stochastic approach to droplet initial conditions was revised.

In the revised approach, Table 1 was changed to Table 2 by modifying the angle range for any droplet size range to better represent the actual range measured. Velocities were retained at the Table 1 values, and, as before, all possible combinations of angle and velocity for a given size range were used, although the number of combinations now depended on drop size, e.g., 28 combinations for the 40-80-μm range, down to four combinations for the 220-μm size. The percentage of fuel associated with droplets in a given size range at a particular angle was obtained using Eq. (13) together with constants taken from Fig. 6. Conservation of liquid mass for the spray was preserved through Fig. 7, and yielded the number of droplets of each size range at each angle. As before, a total of 3000 droplets was used, with shuffling after each 1000.

Figure 8 compares the measured and calculated cumulative volume distributions of the entire break-up region. The calculated cumulative volume distribution is based on a summation across all considered angles for each drop size range. The agreement is acceptable over most of the range, but does reflect some of the truncation made at the larger droplet sizes.

Results

The average drop velocities and angles of trajectory as a function of drop size are shown at the three measurement stations of 3, 6, and 9 cm, in Figs. 9 and 10. Shown on the figures, for reference purposes, are the liquid sheet and air velocities, and the angle of the liquid sheet. The calculations shown were based on the characteristic initial conditions for the droplets. For each drop size, the calculated values of velocity and angle are shown. These are arithmetic averages based on the whole of the computational droplets used in the calculations.

The calculations for droplet velocity indicate that by 3 cm from the injector, droplets with diameters equal to and less than about 35 μm have reached the velocity of the airstream. The measurements suggest that the drop size for terminal velocity at the 3-cm station is about 20 μm. The agreement of measured and calculated velocities is good for droplets of 50-200 μm in diameter at the 3- and 6-cm stations; at the 9-cm station the calculations tend to overestimate the measured velocities by a small amount. The effect of distance is shown for the three droplet sizes of 70, 110, and 170 μm in the crossplot given in Fig. 11. The calculations agree with the data in showing that droplet velocity decreases rapidly with distance for these drop sizes.

The agreements of calculations with measurement in Fig. 10 for droplet angles of trajectory are not as satisfactory as those achieved for velocity. In general, the calculations overestimate the angle, although agreement seems to be improving for droplets above 160 μm. However, the 30-μm droplets, which the calculations have moving at the terminal velocity by 3 cm from the injector, have measured angles in agreement with those calculated for the three axial positions. Despite the poor quantitative agreement, the calculations do reproduce the measured trends, with angle increasing rapidly

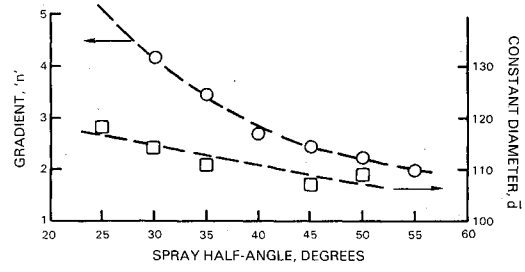

Fig. 6 Variation of droplet size and number with angular position in break-up region represented by Rosin-Rammler distribution.

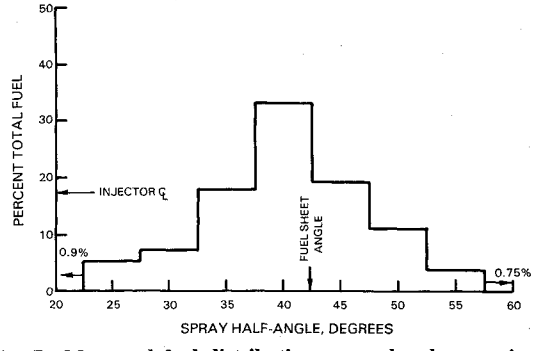

Fig. 7 Measured fuel distribution across break-up region.

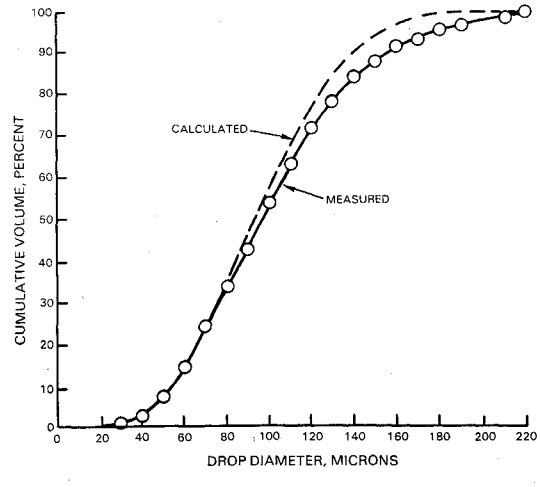

Fig. 8 Comparison of calculated and measured cumulative volume distributions, revised stochastic initial conditions.

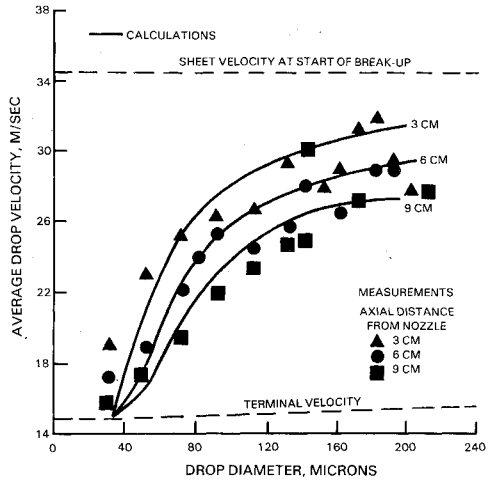

Fig. 9 Variation of average drop velocity with drop size at three downstream positions in the spray.

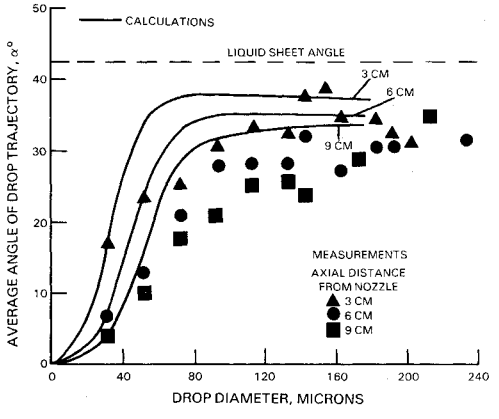

Fig. 10 Variation of average angle of trajectory with drop size at three downstream positions in the spray.

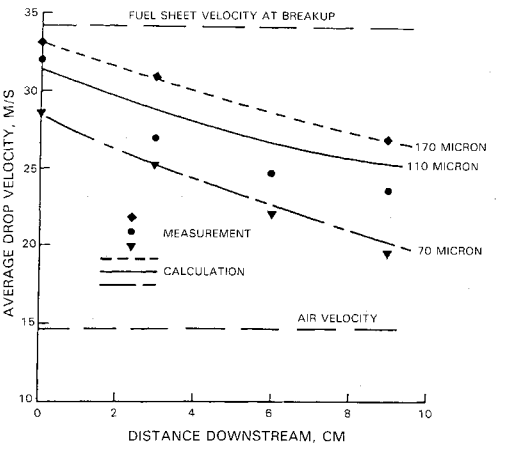

Fig. 11 Variation of average droplet velocity with axial distance from the injector.

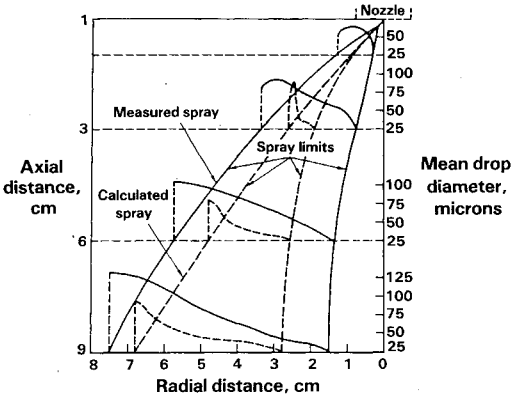

Fig. 12 Variation of mean drop size (based on spatial distribution) with axial and radial positions for characteristic initial conditions.

with drop size to about 70 μm, and for droplets greater than 70 μm in diameter the average angle tending to a constant value or decreasing slightly.

Figure 12 shows calculated and measured variations in mean drop size based on spatial distribution, with axial and radial positions in the spray. In this comparison only the shapes of the distributions should be compared since different techniques were used to obtain these distributions. For the experiment, the distributions are based on the arithmetic mean drop size for the real droplets, obtained at a given position. The wide range of real initial conditions with respect to angle and velocity gives droplets that are spatially dispersed close to the injector. In the calculations, the droplets were assigned a single (characteristic) initial angle and velocity according to their size, following Figs. 2 and 3. Also, the overall level of mean droplet diameter in the calculations was affected by the range of droplet sizes considered. The considered range was 20-180 μm, and it was divided into seven intervals. The actual size range was 10-220-μm droplet diameter.

It can be seen that the shape of the mean size distribution at 9 cm is represented fairly well by the calculations. This downstream distance represents an almost "fully developed" region of the spray where initial conditions are less influential. The well-known tendencies for the smaller droplets to be carried toward the center of a spray through air entrainment while the larger drops migrate toward the edge of the spray under the influence of their inertia seem to be reproduced. The calculated spray width at any station is less than measured, and this could be a direct attribute of the liquid initial condition assumption for the angle.

For the first stochastic droplet initial condition calculation, the mean velocity and angle of trajectory results are not significantly different from those shown in Figs. 9 and 10 for the characteristic initial conditions, and as discussed above. There are some slight improvements in agreement in angles for droplets less than 50 μm. However, there is a marked improvement in the agreement of the calculated and measured spatial distributions of mean drop size, as can be seen when Fig. 13 is compared with Fig. 12. The calculated width of the spray is increased, and the drop size distribution with radius at any axial position is in better agreement with the measured spray.

When the velocity and trajectory calculations with revised stochastic conditions are compared with Figs. 9 and 10, improvements in velocity and angle calculations can be detected for the bigger drops close to the injector. However, these are small. Velocity calculations for the small droplets are worsened for all distances from the injector.

Comparison of Fig. 14 with Fig. 13 shows that the shapes of the spatial distributions of drop sizes are improved at all axial stations. However, the agreements are still far from perfect.

Discussion

The conditions of the experiment and its characteristics indicate that it is an experiment in which droplet information is transmitted only along droplet tracks, and one where other phase interactions are limited to diffusion of droplets by the gaseous phase turbulence.

The spray model used is a trajectory approach, with multidimensional capability and provision for two-way coupling of the phases. The two-way phase coupling used does not permit the droplets to modify the turbulence structure of the continuous phase (standard K-ϵ turbulence model used), but does allow the continuous phase to disperse the droplets through the effect of its turbulence, and for its mean velocity field to be modified by the presence of the droplets. Therefore, it is a model that is more than adequately suited to calculate the experiment under consideration. To relate to the work of Shuen et al.,[20] it is a stochastic separated flow (SSF) method.

The purpose of the study was twofold: First, to check the droplet tracking capability of the model. The work of Shuen et al.[17,18,20,21] and Solomon et al.[19,22] has given encouraging results in this direction for SSF methods. Therefore, the secondary purpose was to explore what might be necessary in the way of specification of liquid initial conditions in order to adequately represent real sprays, initial conditions having been shown to be extremely important in computational fluid dynamics.[20,25]

Droplet trajectories were calculated in Ref. 23 by solving droplet equations of motion for a uniform airstream, with the assumption that all droplets originated from the end of the liquid sheet with the sheet velocity and angle. In effect, this is a simplified version of the characteristic velocity and angle approach adopted presently. The resulting calculations have characteristics similar to those of the present calculations, and relate to the measured data in the same way. However, the quantitative accuracy of the calculations based on the present approach is much improved. The improvement can be attributed to the increased realism in initial conditions provided by making the characteristic angle and velocity functions of drop size. Even so, it is obvious, particularly from Fig. 12, that the characteristic velocity and angle approach is itself not sufficiently realistic.

The introduction of the stochastic approach to initial conditions further increases the realism, and improves the accuracy of the spatial distributions in particular. It is clear when using Monte Carlo techniques such as this, that care has to be taken to ensure truncation does not exert limiting constraints on the solution accuracy. Although the revised

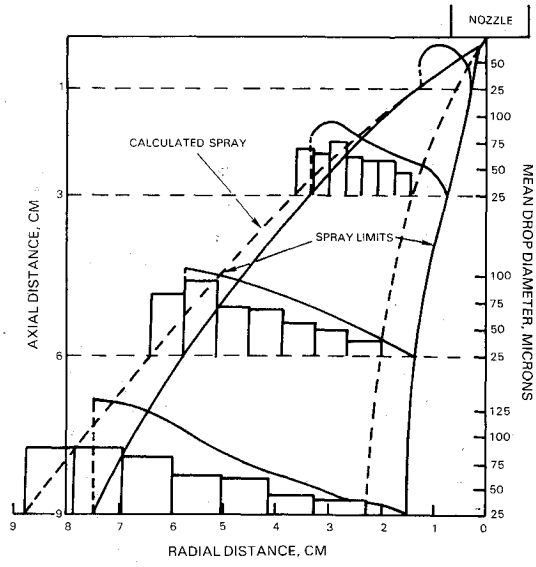

Fig. 13 Variation of mean drop size (based on spatial distribution) with axial and radial positions for stochastic initial conditions.

Table 2 Revised droplet initial conditions for stochastic approach

Drop size range, μm	Droplet angle, deg	Droplet velocity, m/s	Drop size range, μm	Droplet angle, deg	Droplet velocity, m/s
40	25	28	120	30	33
	30	24		35	31
	35	20		40	29
	40	17		45	27
	45			50	
	50		140	30	34
	55			35	32
60	25	32		40	31
	30	28		45	29
	35	24	160	35	34
	40	19		40	33
	45			45	31
	50				30
	55		180	35	34
80	25	32		40	33
	30	29			32
	35	26			31
	40	23	200	40	34
	45				33
	50				32
	55				31
100	25	33	220	40	34
	30	30			33.5
	35	28			32.5
	40	25			32
	45				
	50				

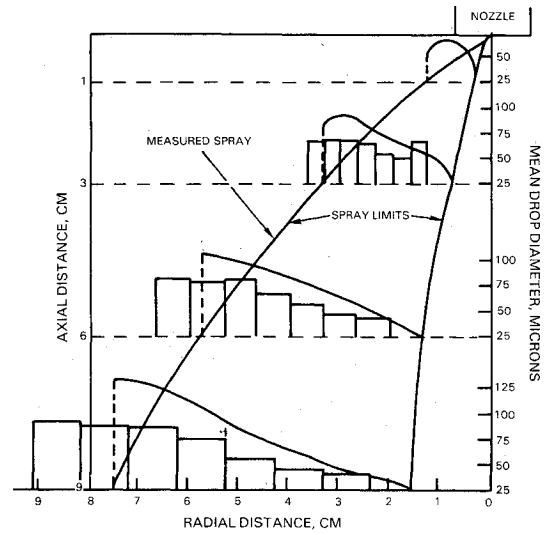

Fig. 14 Variation of mean drop size with axial and radial positions for revised stochastic initial conditions.

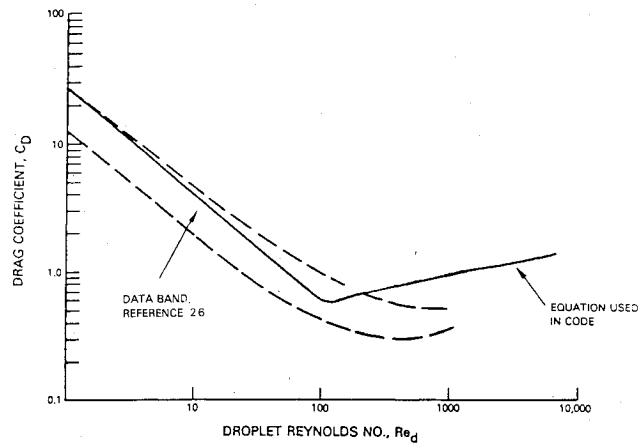

Fig. 15 Drag coefficient information for droplets.

stochastic initial conditions improve the spatial distributions shown in Fig. 14, the cumulative volume distribution for the calculation, Fig. 8, shows that Table 2 really does not have sufficient representation for the larger drops. This is reflected in the levels calculated for the mean drop sizes in Fig. 14. The implementation of the technique, as exemplified by Table 2, was governed by the way the computer code for the spray model was originally written. A more satisfactory method would result if the code was rewritten so that the full Rosin-Rammler distributions could be used directly in the calculation, rather than the reduced representation of Table 2. Truncation effects would then be avoided. It is apparent that adequate specification of droplet initial conditions is of prime importance in determining the accuracy of droplet spatial distributions.

The agreement of the calculations with measurements for drop velocity does not change substantially as the droplet initial conditions are changed. The agreement improves with distance from the injector, Fig. 9. The agreement with the data is of similar order to that achieved in Ref. 22 for non-evaporating liquid sprays using Shuen's SSF spray model, where it was also observed that agreement improved with distance from the injector. In Ref. 22, initial conditions were carefully measured at 50 injector diameters from injection. These measured conditions were detailed and extensive, and covered mean and fluctuating velocities for both liquid and gaseous phases, as well as drop size distributions. The agreement with measurement for the present calculated angles of trajectory also improves with distance from the injector, Fig. 10. These observations altogether suggest that droplet initial conditions alone are not the major contributor to the discrepancy in droplet trajectory calculations.

Setting to one side any shortcomings that might exist in the experiment, the reasons for the poor agreements in calculated droplet trajectories could be associated with physical aspects: the droplet drag law, neglect of drop-drop interactions, and neglect of turbulence modification.

Since the spray is dilute and has low loading, turbulence modification in the gaseous phase by the droplets should not be of major importance. This is on an overall basis, but might not be applicable extremely close to the injector. However, Shuen's model[20] does account for such turbulence modification, but has shown the same trends as the present model. In any case, gas-phase turbulence is not of great importance in the experiment. Therefore, turbulence modification is probably not the cause.

The droplet drag law[9] used in the calculations is a composite one attempting to cover accelerating spheres, evaporating droplets, and burning droplets. It is derived from experiments that cover a diverse range of operating conditions and studies, and was chosen because it included burning sprays. It is not a law in which great faith can be held. Figure 15 compares this law with the data of Yuen and Chen[26] for evaporating liquid droplets. The change in sign of the slope of the law to a positive value for drop Reynolds numbers over 100 is to match the burning droplet data as close as possible. However, for droplet Reynolds numbers less than 100, the law is in fair agreement with the data of Yuen and Chen. For the present conditions, a Reynolds number around 100 approximates to droplets in the 50-120-μm-diam size range.

Figure 10 indicates that in the calculations droplets in the 50-μm-diam range appear to have incorrect drag. It is tempting to assign the discrepancies in angle of trajectory calculations to the drag law used. Certainly, knowledge of droplet drag is not reliable close to the injector where drop-drop interactions are important. However, in order to improve the drag laws, extremely difficult in situ measurements of sprays will be necessary.

It has been demonstrated that extensive knowledge is required of the droplet initial conditions in a spray in order to make adequate calculations. Known experimental information has to be used to set up Monte Carlo procedures for such initial conditions. Clearly, it is necessary to be able to somehow analytically derive this information in order to make a priori calculations. Equally clearly, it is impossible to describe analytically the liquid sheet break-up process. Therefore, it will be necessary to make detailed experimental studies of the break-up processes of different fuel injector designs to see if empirical general descriptions can be obtained for each class of fuel injector.

Conclusions

A standard TEACH-type numerical technique using familiar, state-of-the-art physical modeling, including a Lagrangian spray model for liquid fuels, has been applied to a hollow-cone pressure atomizer spraying water into a coflowing confined airstream. The study was limited to the particle-tracking aspects of the model, and investigated the requirements of liquid initial condition specification in order to adequately represent the spray. The following conclusions can be drawn.

1) Calculation of droplet trajectories depends on both specification of initial conditions for the spray and the drag law used for the droplets.

2) Correct calculations of spatial distributions of droplets in the spray, especially in the near field, are strongly dependent on the specification of liquid initial conditions.

3) Specification of a single liquid initial angle and velocity for all drop sizes, or a characteristic single liquid initial angle and velocity as a function of drop size, does not provide sufficient information to yield acceptable calculations of droplet spatial distribution.

4) Real sprays are not always completely random, and it is important that any such biasing be reflected in the Monte Carlo representation of the spray origin. Sufficient information is not known about real sprays to be able to do this a priori.

5) Experiments are required for the following: a) Improved drag law reflecting the presence of other droplets. b) Benchmark test of turbulent dispersion of droplets. c) Study and characterization of the liquid sheet break-up process.

References

[1]Gosman, A. D. and Ideriah, F. T. K., "TEACH-2E: A General Computer Program for Two-Dimensional, Turbulent, Recirculating Flows," Imperial College, London, England, Mechanical Engineering report (unnumbered), June 1976.

[2]Sturgess, G. J., "Aerothermal Modeling—Phase I, Final Report," NASA CR-168202, May 1983.

[3]Megdal, D. and Agosta, V. D., *Applied Mechanics*, Vol. 35, 1967, pp. 860-865.

[4]Crowe, C. T., "Gas-Droplet Flow Field in the Vicinity of an Atomizer," 11th JANNAF Combustion Meeting, Sept. 1974.

[5]Buckingham, A. C. and Siekhaus, W. J., "Interaction of Moderately Dense Particle Concentrations in Turbulent Flow," AIAA Paper 81-0346, Jan. 1981.

[6]Crowe, C. T., Sharma, M. P., and Stock, D. E., "The Particle-Source-In-Cell (PSI-Cell) Model for Gas-Droplet Flow," ASME Paper 75-WA/HT-25, 1975; also, *Journal of Fluids Engineering*, Vol. 99, 1977, pp. 325-332.

[7]Lockwood, F. C., Salooja, A. P., and Syed, S. A., "A Prediction Method for Coal-Fired Furnaces," *Combustion and Flame*, Vol. 38, 1980, pp. 1-15.

[8]Soo, S. L., *Fluid Dynamics of Multiphase Systems*, Blaisdell Publishing Co., Waltham, MA, 1967.

[9]Williams, A., "Combustion of Droplets of Liquid Fuels: A Review," *Combustion and Flame*, Vol. 21, 1973, pp. 1-31.

[10]Elghobashi, S. E. and Abou-Arab, T. W., "A Second-Order Turbulence Model for Two-Phase Flows," 7th International Heat Transfer Conference, Sept. 1982.

[11]Gosman, A. D. and Ioannides, E., "Aspects of Computer Simulation of Liquid-Fueled Combustors," AIAA Paper 81-0323, Jan. 1981.

[12]Faeth, G. M., "Current Status of Droplet and Liquid Combustion," *Progress in Energy and Combustion Science,* Vol. 3, 1977, pp. 191-224.

[13]Banhawy, Y. El and Whitelaw, J. H., "Assessment of an Approach to the Calculation of the Flow Properties of Spray Flames," *Proceedings of the AGARD Symposium on Combustor Modelling,* AGARD CP 275, Oct. 1979, pp. 12.1-12.11.

[14]Banhawy, Y. El and Whitelaw, J. H., "Experimental Study of the Interaction Between a Fuel Spray and Surrounding Combustion Air," *Combustion and Flame,* Vol. 42, 1981, pp. 253-275.

[15]Mahallway, F. M. El, Khalil, E. E., and Abdel, Aal O., "Experimental and Numerical Investigation of a Large Cylindrical Oil-Fired Combustor," ASME Paper 83-GT-184, 1983.

[16]Boysan, F., Ayers, W. H., Swithenbank, J., and Pan, Z., "Three-Dimensional Model of Spray Combustion in Gas Turbine Combustors," AIAA Paper 81-0324, Jan. 1981.

[17]Shuen, J. S., Chen, L. D., and Faeth, G. M., "Evaluation of a Stochastic Model of Particle Dispersion in a Turbulent Round Jet," *AIChE Journal,* Vol. 29, 1983, pp. 167-170.

[18]Shuen, J. S., Chen, L. D., and Faeth, G. M., "Predictions of the Structure of Turbulent, Particle-Laden, Round Jets," AIAA Paper 83-0066, Jan. 1983.

[19]Solomon, A. S. P., Shuen, J. S., Zhang, Q. F., and Faeth, G. M., "Measurements and Predictions for Non-evaporating Sprays in a Quiescent Environment," AIAA Paper 83-0151, Jan. 1983.

[20]Shuen, J. S., Solomon, A. S. P., Zhang, Q. F., and Faeth, G. M., "A Theoretical and Experimental Study of Turbulent Particle-Laden Jets," NASA CR-168293, Nov. 1983.

[21]Shuen, J. S., Solomon, A. S. P., Zhang, A. F., and Faeth, G. M., "Structure of Particle-Laden Jets: Measurements and Predictions," AIAA Paper 84-0038, Jan. 1984.

[22]Solomon, A. S. P., Shuen, J. S., Zhang, Q. F., and Faeth, G. M., "Structure of Non-evaporating Sprays: Measurements and Predictions," AIAA Paper 84-0125, Jan. 1984.

[23]Mellor, R., Chigier, N. A., and Beer, J. M., "Hollow-Cone Liquid Spray in Uniform Air Stream," *Proceedings of the Symposium on Combustion and Heat Transfer in Gas Turbine Systems,* edited by E. R. Norster, Cranfield International Symposium Series, Vol. 11, Pergamon Press, Oxford, 1971, pp. 291-305.

[24]Simmons, H. C., "The Correlation of Drop-Size Distribution in Fuel Nozzle Sprays," *Journal of Engineering for Power,* Vol. 99, No. 3, 1977, pp. 309-319.

[25]Sturgess, G. J., Syed, S. A., and McManus, K. R., "Importance of Inlet Boundary Conditions for Numerical Simulation of Combustor Flows," AIAA Paper 83-1263, June 1983.

[26]Yuen, M. C. and Chen, L. W., "On Drag of Evaporating Liquid Droplets," *Combustion Science and Technology,* Vol. 14, 1976, pp. 147-154.

From the AIAA Progress in Astronautics and Aeronautics Series...

SHOCK WAVES, EXPLOSIONS, AND DETONATIONS—v. 87
FLAMES, LASERS, AND REACTIVE SYSTEMS—v. 88

Edited by J. R. Bowen, University of Washington,
N. Manson, Université de Poitiers,
A. K. Oppenheim, University of California,
and R. I. Soloukhin, BSSR Academy of Sciences

In recent times, many hitherto unexplored technical problems have arisen in the development of new sources of energy, in the more economical use and design of combustion energy systems, in the avoidance of hazards connected with the use of advanced fuels, in the development of more efficient modes of air transportation, in man's more extensive flights into space, and in other areas of modern life. Close examination of these problems reveals a coupled interplay between gasdynamic processes and the energetic chemical reactions that drive them. These volumes, edited by an international team of scientists working in these fields, constitute an up-to-date view of such problems and the modes of solving them, both experimental and theoretical. Especially valuable to English-speaking readers is the fact that many of the papers in these volumes emerged from the laboratories of countries around the world, from work that is seldom brought to their attention, with the result that new concepts are often found, different from the familiar mainstreams of scientific thinking in their own countries. The editors recommend these volumes to physical scientists and engineers concerned with energy systems and their applications, approached from the standpoint of gasdynamics or combustion science.

Published in 1983, 505 pp., 6×9, illus., $39.00 Mem., $59.00 List
Published in 1983, 436 pp., 6×9, illus., $39.00 Mem., $59.00 List

TO ORDER WRITE: Publications Order Dept., AIAA, 1633 Broadway, New York, N.Y. 10019